IEEE Photonics Journal
An IEEE Photonics Society Publication

Open Access

High-Performance GeSn Photodetector Covering All Telecommunication Bands

Volume 13, Number 2, April 2021

Nan Wang
Chunlai Xue
Fengshuo Wan
Yue Zhao
Guoyin Xu
Zhi Liu
Jun Zheng
Yuhua Zuo
Buwen Cheng
Qiming Wang

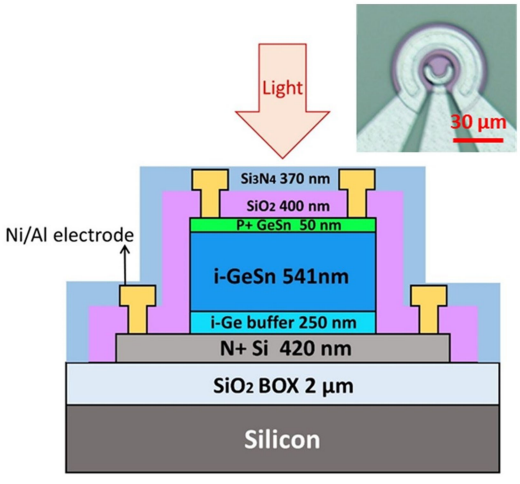

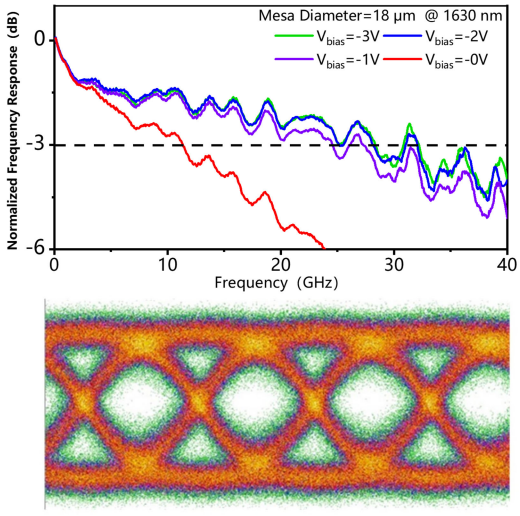

40 Gpbs 18 μm -3 V @1630 nm

DOI: 10.1109/JPHOT.2021.3065223

High-Performance GeSn Photodetector Covering All Telecommunication Bands

Nan Wang,[1,2] Chunlai Xue,[1,2] Fengshuo Wan,[1,2] Yue Zhao,[1,2] Guoyin Xu,[1,2] Zhi Liu,[1,2] Jun Zheng,[1,2] Yuhua Zuo,[1,2] Buwen Cheng,[1,2] and Qiming Wang[1,2]

[1]State Key Laboratory on Integrated Optoelectronics, Institute of Semiconductors, Chinese Academy of Sciences, Beijing 100083, China
[2]Center of Materials Science and Optoelectronics Engineering, University of Chinese Academy of Sciences, Beijing 100049, China

DOI:10.1109/JPHOT.2021.3065223

Manuscript received January 11, 2021; revised March 1, 2021; accepted March 7, 2021. Date of publication March 11, 2021; date of current version March 31, 2021. This work was supported in part by the National Natural Science Foundation under Grants 61874109, and 61774143, and in part by the Key Research Program of Frontier Sciences, CAS under Grant ZDBS-LY-JSC008. The work of Chunlai Xue was supported by the National Key Research and Development Program of China under Grants 2017YFA0206404 and 2017YFF0104803. Corresponding author: Chunlai Xue (e-mail: clxue@semi.ac.cn).

Abstract: We report the design and fabrication of a high-speed GeSn normal-incidence p-i-n photodetector. To realize high-speed detection in all telecommunication bands, we optimize the Sn content in the absorption layer, the absorption-layer thickness, and the device size. The responsivity of the 18-μm-diameter device at 1550 nm reaches 0.32 A/W with an extended cutoff wavelength of 1700 nm and a 3-dB bandwidth as high as 28 GHz under -3 V bias, clear open eye diagrams are also obtained under zero bias at 1630 nm. All the results indicate that the device has a significant potential for applications in Si-based optical telecommunication in all telecommunication bands.

Index Terms: Germanium alloys, integrated optoelectronics, optical interconnections, photodetectors.

1. Introduction

Silicon photonics is widely recognized as the prime solution for optical interconnects for data communication. Likewise, Ge is regarded as the ideal absorber for detectors used in silicon photonics due to its compatibility with the current complementary metal-oxide semiconductor (CMOS) technology and its strong absorption from 1.3 to 1.55 μm. In addition, state-of-the-art Ge detectors typically have a 30–70 GHz bandwidth in the C band (1.53–1.565 μm) [1]. However, the rapid development of database applications and mobile networks demands higher communication capacity. Improving data transmission bandwidth thus requires the development of Si-based photodetectors that cover all telecommunication bands for wavelength-division-multiplexing technology. However, Ge is an indirect-bandgap semiconductor with a bandgap of 0.805 eV, and the responsivity of Si-based Ge photodetectors decreases dramatically above 1.55 μm, so that these devices can't cover the L-band (1.565–1.625 μm) or U-band (1.625–1.675 μm) telecommunication windows.

Fortunately, the GeSn alloy with a tunable bandgap from 0.8 to 0 eV shows great potential for developing photodetectors that cover all telecommunication bands, and its group-IV compounds

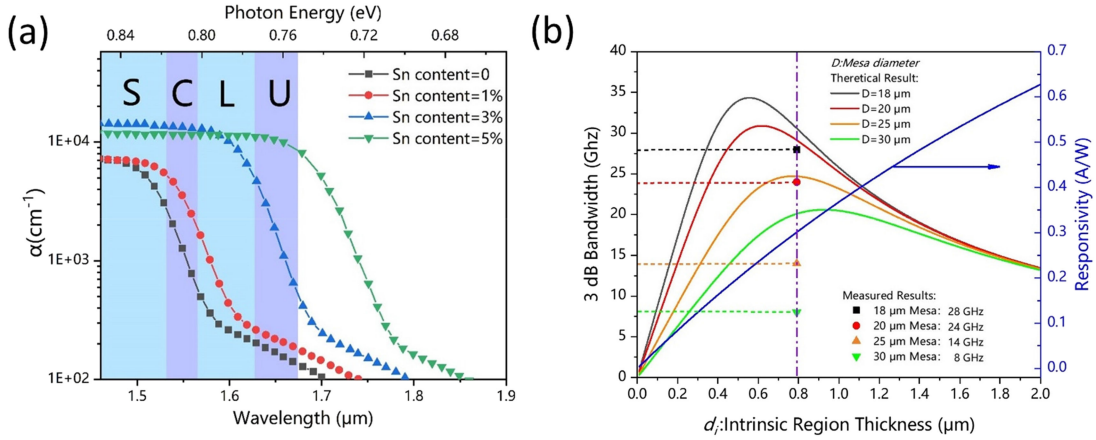

Fig. 1. (a) Absorption coefficient of GeSn alloys with different Sn content [12], [13]. (b) Calculated responsivity, and 3-dB bandwidth versus thickness of the intrinsic layer for device diameters ranging from 12 to 30 μm. Also shown is the measured 3-dB bandwidth for a 0.79-μm-thick device of varying bandwidth (8–28 GHz).

are compatible with the current CMOS technology [2], [3]. Over the past decades, the breakthrough in fabricating high-quality GeSn films on Si substrates has led to GeSn photodetectors with a cutoff wavelength around 3.65 μm for short-wave and mid-wave infrared detection [4]–[8], while few efforts have been devoted to fabricating high-speed GeSn photodetectors for tele- and data communication.

To work toward GeSn tele and data communication devices, we report herein the design and fabrication of a high-speed GeSn photodetector. To obtain a high-frequency response, low dark current, and easy fiber coupling, the photodetector is fabricated as a normal-incidence p-i-n structure [9]–[11]. Meanwhile, the Sn content of the GeSn alloy, the absorption-layer thickness, and the size of the mesa of the photodetector are all optimized to balance cutoff wavelength, dark current, responsivity, and bandwidth. The result for an 18-μm-diameter device at room-temperature is a responsivity from 0.32 to 0.19 A/W at 1.55 and 1.63 μm, respectively, with an extended photodetection range of 1.7 μm and a 28 GHz 3-dB bandwidth. These results reflect the potential of these devices in Si-based optical telecommunications.

2. Device Design Issues

A p-i-n photodetector is a diode with a wide, undoped intrinsic semiconductor region sandwiched between a p-type and an n-type semiconductor region. The most significant merits of these devices are the cutoff wavelength, dark current, and speed. In this work, to be able to have a high photo response in all telecommunication bands, GeSn alloy is grown on Ge-buffered silicon-on-insulator (SOI) to serve as the absorption layer of the device. With increasing Sn content, the bandgap of GeSn alloy decreases and the GeSn-alloy absorption spectrum redshifts [Fig. 1(a)] [4], [12], [14], resulting in the redshift of the photodetector cutoff wavelength. However, the low solubility of Sn in Ge matrix requires the non-equilibrium growth of GeSn film under low growth temperature, the higher Sn content in GeSn films is, the lower the critical growth temperature are required. The low growth temperature results in high defect density in the GeSn absorption layer, leading to a greater dark current in GeSn-based photodetectors [15].

Thus, we must strike a balance between the cutoff wavelength and the dark current in these devices. Fig. 1(a) shows the absorption spectrum of GeSn alloy for several Sn contents [12], [13], which redshifts with increasing Sn content. For GeSn alloy with 3% Sn content, the absorption

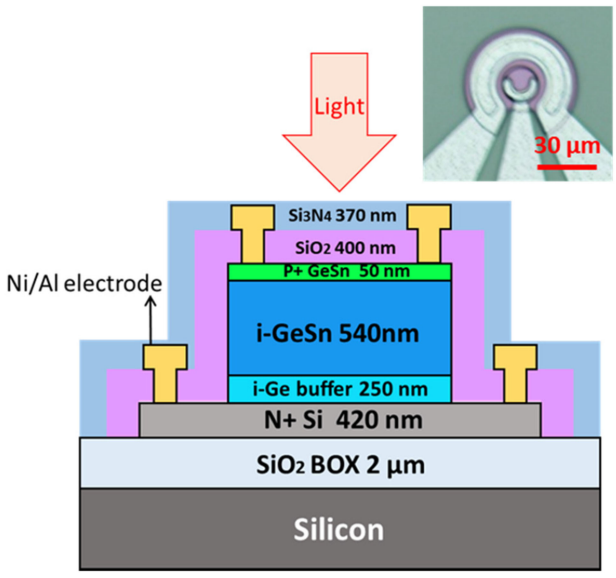

Fig. 2. Schematic cross-sectional view of GeSn on SOI detector. The inset shows an optical micrograph of the device (top view).

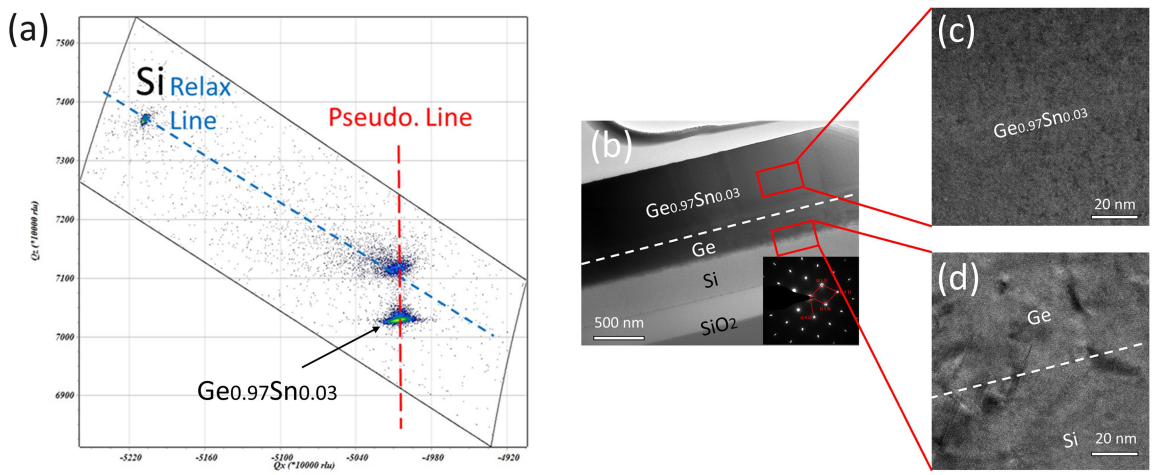

Fig. 3. (a) XRD-RSM of the $(-2\ -24)$ plane of $Ge_{0.97}Sn_{0.03}$ sample grown on Ge-buffered SOI substrate. (b) Cross-sectional TEM image of $Ge_{0.97}Sn_{0.03}$ sample. Inset shows results of selected-area electron diffraction. (c), (d) High-resolution transmission electron micrograph corresponding to red boxes in panel (b).

spectrum covers all telecommunication bands. Thus, we use the GeSn alloy with 3% Sn content as the absorption layer of the detector.

The responsivity of a normal-incidence p-i-n detector measures the electrical output per unit optical input and can be expressed as [9], [16]

$$\mathrm{R} = \frac{q}{hf}\eta_{ex} \approx \frac{\lambda\,(\mu m)}{1.24\ (\mu m \times W/A)}\,\eta_{ex} = \frac{\lambda\,(\mu m)}{1.24\,(\mu m \times W/A)}\,(1-\theta_R)\,\eta_{in}\left(1-e^{-\alpha d_i}\right), \tag{1}$$

where q is the electron charge, f is the frequency of the optical signal, h is Planck's constant, λ is the vacuum wavelength, η_{ex} is the external quantum efficiency, θ_R is the reflectivity due to the

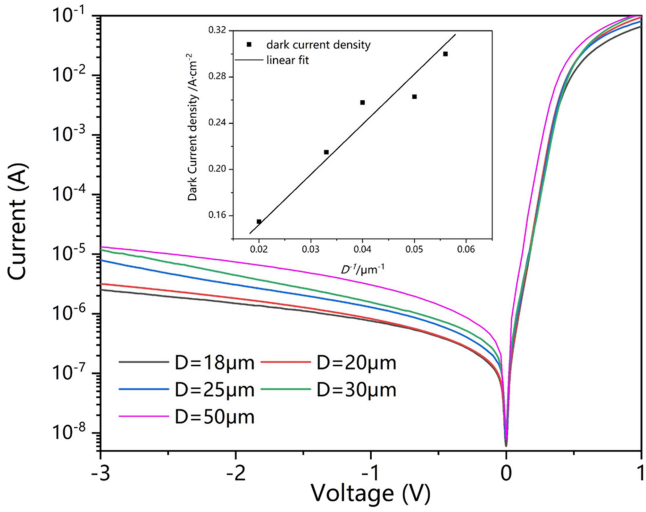

Fig. 4. Typical I-V characteristics of device (device diameter D = 18, 20, 25, 30, and 50 μm). The inset shows the dark current density versus 1/D at −1 V bias.

Fresnel-index mismatch at the input interface and is set to zero to simplify the calculation, η_{in} is the internal quantum efficiency, α is the optical absorption coefficient (in this work, in order to simplify the calculation, and considering the low Sn content in Ge matrix, we use the absorption coefficient of pure Ge '3485 cm^{-1}' in the calculation), and d_i is the absorption-layer thickness.

The electrical 3-dB bandwidth of a photodetector specifies the frequency range from dc to the cutoff frequency f_{3dB}. For a normal-incidence p-i-n photodetector, this bandwidth is mainly determined by the carrier transit-time-limited bandwidth f_T and the resistor-capacitor bandwidth f_{RC} in the intrinsic layer. The frequencies f_T , f_{RC}, and f_{3dB} can be approximated by using [9], [10]

$$f_T \approx \frac{0.45 v_{sat}}{d_i}, \quad f_{RC} = \frac{1}{2\pi (R_L + R_s) C}, \quad f_{3dB} = \sqrt{\frac{1}{f_T^{-2} + f_{RC}^{-2}}}, \tag{2}$$

where v_{sat} is the saturated-hole velocity (because the saturation velocity of GeSn is not known, we approximate it as that of pure Ge, 6×10^4 m/s), C is the capacitance of the device, which can be calculated by using $C = \varepsilon A / d_i$, where ε is the permittivity of the absorption region ($\varepsilon_{Ge} = 16.2$), A is the area of device mesa, R_L is the load resistance (50 Ω in this work), and R_S is the series resistance.

Fig. 1(b) plots the calculated responsivity (right axis) and 3-dB bandwidth (left axis) as functions of the thickness d_i of the absorption layer for devices of differing diameters. Also plotted are several measurements of the 3-dB bandwidth for 0.79-μm-thick devices of varying bandwidth. The results reveal that a high-bandwidth is achieved with a thin intrinsic layer and a small mesa. However, the core diameter of a single mode optical fiber is around 9 to 10 μm, it requires the diameter of device photosensitive surface to be larger than 10 μm. If not, the light from optical fiber can't be fully coupled into device; meanwhile, the small mesa size makes the fiber alignment a difficulty. In this work, in order to ensure the sufficient tolerance for fiber alignment, we select a minimum device size of 18 μm. Meanwhile, to guarantee a responsivity around 0.3 A/W at 1550 nm, we choose an absorption-layer thickness of 790 nm for the device

3. Material Growth and Device Fabrication

The sample was grown by solid-source molecular beam epitaxy on a SOI substrate with a 420-nm-thick n + Si(001) layer and a 2-μm-thick buried oxide layer. The epitaxial structure consists of (a)

a Ge buffer grown by the two-step method and composed of a 70 nm low-temperature layer and an 180 nm high-temperature layer, followed by five annealing cycles between 600 and 800 °C to improve the crystalline quality; (b) a 540 nm $Ge_{0.97}Sn_{0.03}$ intrinsic layer grown at 200 °C; and (c) a 50 nm in-su doping P + $Ge_{0.97}Sn_{0.03}$ layer at 200 °C. Boron serves as dopant, and the doping concentration is 1×10^{19} cm^{-3}.

The GeSn p-i-n detectors were designed as double-mesa structures and realized by photolithography and inductively-coupled-plasma (ICP) etching. The first mesa process defines the diameter of the photodetectors and the second one isolates the photodetectors. After etching the mesas, a 400-nm-thick SiO_2 passivation layer was deposited by plasma-enhanced chemical vapor deposition (PECVD). Next, the contact hole was etched through the SiO_2 by dry etching and wet etching; following which the metal electrodes were formed from 50 nm Ni and 300 nm Al. A 370-nm-thick Si_3N_4 layer was then deposited by PECVD to reduce the surface reflection and protect the metal electrode. Finally, the pad holes on the metal electrodes were opened by ICP etching. Fig. 2 shows a cross-sectional view of the device, and the inset shows an optical micrograph of an 18-μm-diameter device.

To verify the concentration of Sn and the strain in the GeSn layer, we plot in Fig. 3(a) the X-ray diffraction reciprocal space mapping (XRD-RSM) around the asymmetric (−2 −24) reflection. The GeSn layer and the Ge buffer layer have the same in-plane lattice constant, revealing that the GeSn layer grown on the Ge buffer is pseudomorphical. The Sn content and stain is 3.2% and −0.46%, respectively, as calculated from the RSM data. In addition, the cross-sectional transmission electron micrograph of the epitaxial layer shown in Fig. 3(b) reveals a few threading dislocations and defects in the Ge buffer layer that are limited to the low-temperature Ge layer, demonstrating the high crystalline quality of the GeSn layer and the high-temperature Ge layer. These results are consistent with the high-resolution transmission electron micrographs shown in Fig. 3(c) and 3(d). The inset in Fig. 3(b) shows selected-area electron diffraction of the interface between GeSn and the Ge buffer, which also evinces the single-crystalline nature of the GeSn film.

4. Device Characteristics

The room-temperature current-voltage (*I-V*) characteristics of the GeSn detectors were obtained by using an Agilent B1500A Semiconductor Device Analyzer. Fig. 4 shows the dark *I-V* characteristics of the fabricated GeSn p-i-n photodetectors with different mesa diameters *D*. The devices exhibit remarkable rectification with a high on-off current ratio (I_{on}/I_{off}) near 5×10^5 between 1 and −1 V, which manifesting excellent rectifying behavior. The series resistance, which can be calculated from the forward *I-V*, is as small as 5–9 Ω and is indicative of good ohmic-contact in the device. The 18-μm-diameter device has a dark current of 759 nA at −1 V, which corresponds to a dark-current density $J_{total} = 0.30$ A/cm^2. The dark-current density can be divided into a bulk current density J_{bulk} and a surface-leakage current density J_{surf} as follows:

$$J_{total} = J_{bulk} + \frac{4J_{surf}}{D}, \tag{3}$$

where *D* is the device diameter. The inset in Fig. 4 shows the total dark-current density of various devices versus 1/*D*. (3) gives J_{bulk} and J_{surf} as 0.0656 A/cm^2 and 0.0001 A/cm, respectively. Given that J_{bulk} is proportional to the threading-dislocation density, a small J_{bulk} is indicative of high crystalline quality in the epitaxial GeSn layer.

The room-temperature optical responsivity of the GeSn photodetectors was measured with an Agilent B1500A semiconductor parameter analyzer, a probe station, and a tunable laser. Light was coupled into the top surface of the devices via a single-mode fiber probe. The laser output was measured by using a calibrated reference detector. The spectral response of the photodetector was measured by using a Nicolet 6700 Fourier transform infrared spectrometer with a KBr beam splitter and glow-bar source at room-temperature. A commercial InGaAs photodetector was used to calibrate spectral responsivity.

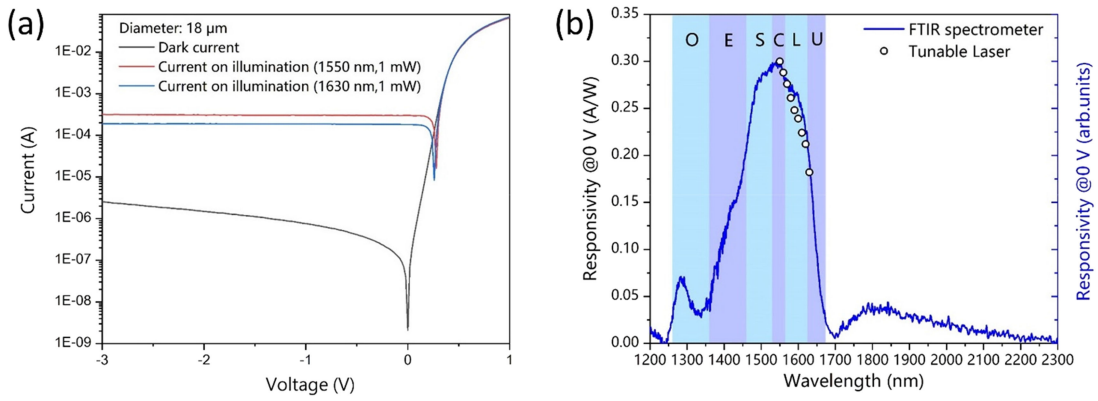

Fig. 5. (a) I-V characteristics of device with and without illumination. The device diameter is 18 μm, the optical power is 1 mW, the wavelength of the incident light is 1550 and 1630 nm. (b) Optical responsivity and spectrum response of the device at 0 V.

Fig. 5(a) shows the current of a device with and without illumination. At a reverse bias of -3 V, the device shows a responsivity of 0.32 and 0.19 A/W at 1550 and 1630 nm, respectively. The saturation of the optical responsivity already at 0 V bias reveals that the photodetector configuration allows for complete photogenerated-carrier collection without bias. Fig. 5(b) shows the photocurrent responsivity spectrum of the GeSn photodetector under zero bias; a scatter plot measured by a 1550–1630 nm tunable laser is also shown in Fig. 5(b) for comparison. These results show that the cutoff wavelength of the device is extended to 2080 nm with the incorporation of Sn, which matches well with the calculated bandgap of 0.61eV with 6-band k·p band model and the deformation potential theory [17], [18]. However, the vertical resonant cavity structure formed with the top Si_3N_4, SiO_2 passivation layer and the buried SiO_2 layer results in the photo responsivity fluctuations in the responsivity spectrum [8], and resonance responsivity peaks (1280, 1550 and 1830 nm) and troughs (1340 and 1700 nm) are confirmed. The trough at 1700 nm causes the low responsivity, so that the photo response range of the detector can cover the C, L and most of U telecom bands.

The optoelectronic frequency response of GeSn photodetectors was measured on-wafer by using an Agilent Lightwave component analyzer with a 50 Ω GSG RF probe. Fig. 6(a) shows details of the measurement setup. Fig. 7(a) shows the normalized frequency response of an 18-μm-diameter device at 1550 and 1630 nm. Illumination of the 18-μm-diameter device at 1550 and 1630 nm produces basically identical 3-dB bandwidths, indicative of a device with strong responsivity at both 1550 and 1630 nm. At low reverse bias, the intrinsic region of the device is not fully depleted, and the undepleted intrinsic region slows the transit of photogenerated carriers, leading to low bandwidth, but at a bias of -3V, a 3-dB bandwidth of 28 GHz is achieved in 18-μm-diameter device. For comparison, the measurement results of responsivity, bandwidth, and dark current density of the reported NI GeSn photodetectors are listed in Table 1 [19]–[23]. To our knowledge the device proposed in this work prohibit the best comprehensive performance in C, L and U communication bands among the reported NI GeSn photodetectors. It's worth to notice that Michal Oehme et. al. realized a GeSn NI photodetectors with a bandwidth of 40 GHz, but the cost is a small device diameter (5 μm), which is much smaller than the core diameter of single mode optical fiber, and when the diameter of their GeSn photodetectors rises to 20μm, the bandwidth decrease dramatically (5 GHz) and much smaller than the device with same size reported in this work (20 GHz).

Fig. 7(b) shows the normalized frequency response of devices with increasing diameters at -3 V. The 3-dB bandwidth decreases with increasing device diameter, which is consistent with the calculation. However, the measured 3-dB bandwidths of devices with different mesa diameters

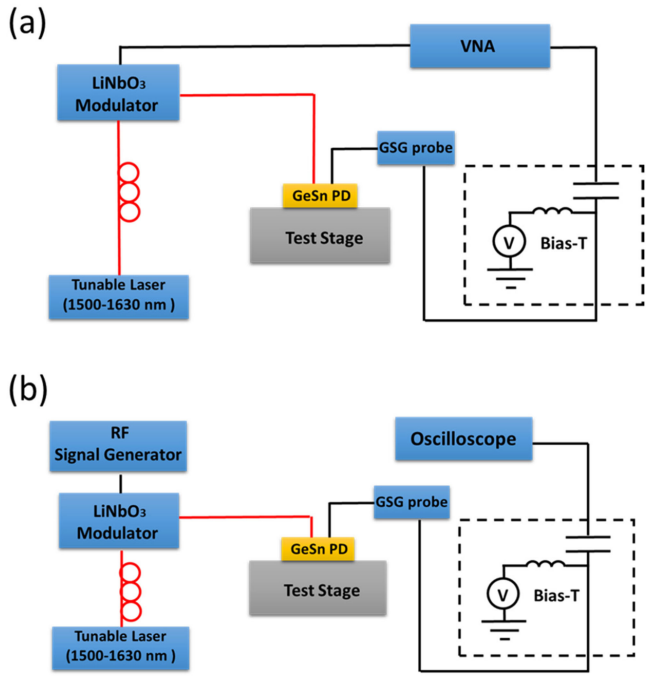

Fig. 6. Schematic illustration of measurement setup for (a) 3-dB bandwidth and (b) eye diagram.

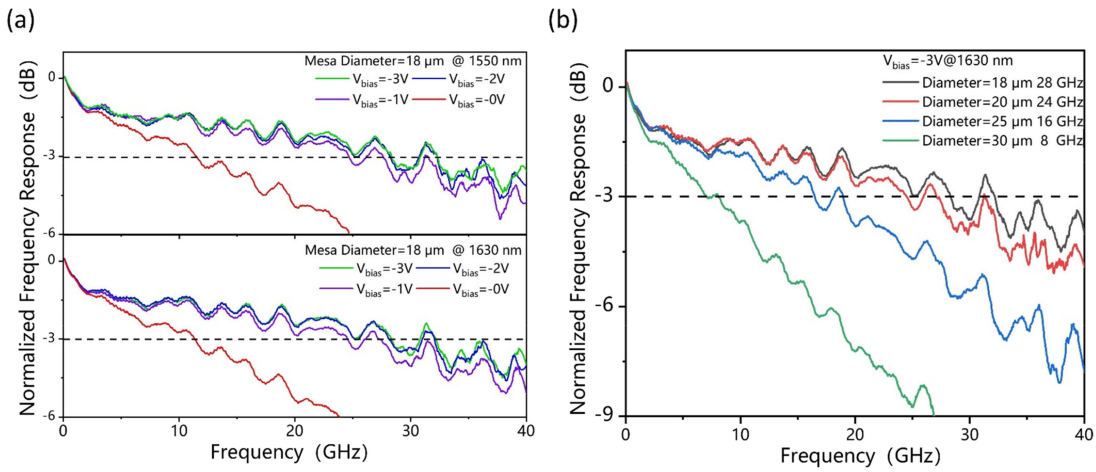

Fig. 7. (a) Normalized frequency response of 18-μm-diamter device at 1550 and 1630 nm. (b) Normalized frequency response of device with various diameters at 1630 nm.

fall below the theoretical results, which may be due to the ohmic-contact resistance of the pad electrodes and the parasitic capacitance of the device.

An on-wafer measurement of the eye diagram served to investigate the data transmission characteristics of the device. Fig. 6(b) details the measurement setup, and Fig. 8 shows the eye diagrams of GeSn photodetectors with diameters ranging from 18 to 25 μm at 0, -1, and -3 V. Clear, open eye diagrams are obtained from all photodetectors except for the 25-μm-diameter photodetector, even at 0 V, indicating the GeSn photodetectors have great potential as low-power-consumption receivers for high-speed data transmission. With increasing photodetector diameter, the eyes become slightly narrower, reflecting the decreasing bandwidth and which is consistent

TABLE 1
Overview of Performance Obtained By GeSn Top-Illuminated Photodetector

First author	Responsivity @ 1550 nm (A/W)	3-dB bandwidth (GHz)	Dark current density @ −1V (A/cm^2)	Year
Michael Oehme [19]	0.218	40 @1550 nm (5 μm) 5@1550 nm (20 μm)	0.892	2014
Yuan Dong [20]	0.216	1.2 @ 2000 nm (20 μm)	0.031	2017
Shengqiang Xu [21]	0.214	10 @ 2000 nm (20 μm)	0.045	2019
Huong Tran [22]	0.18	1.78 @ 2000 nm (100 μm)	30	2019
Hao Zhou [23]	0.307	12 @ 2000 nm (30 μm)	0.016	2020
This work	**0.32**	**28 @ 1550 nm and 1630 nm (18 μm)**	**0.30**	**This work**

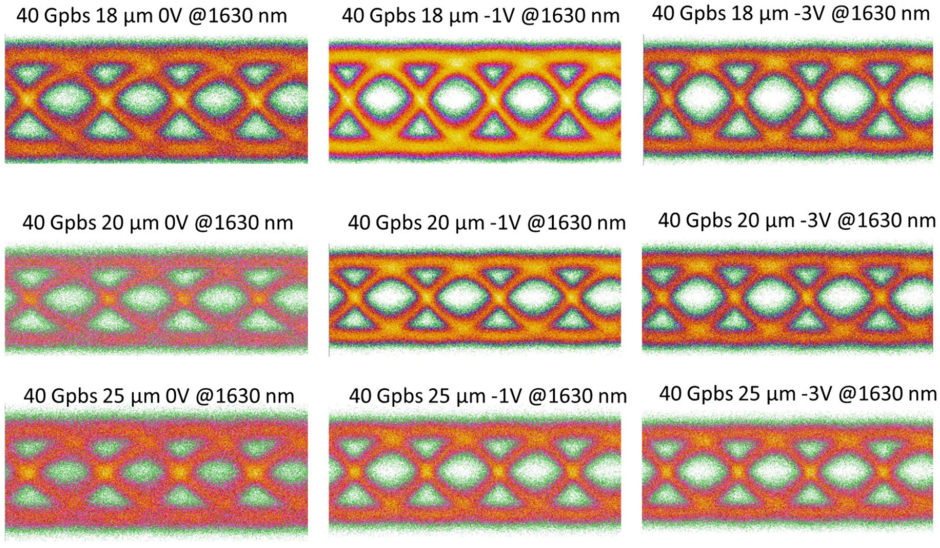

Fig. 8. 40 Gbps eye diagrams of devices with increasing diameters (D = 18, 20, 25 μm) at 0, −1, −3 V.

with the calculation. Upon increasing the reverse bias, the eyes open wider, but once the reverse bias exceeds −1 V, the eye diagrams remain constant, indicating that the intrinsic region of the photodetector is almost depleted at −1 V.

5. Conclusion

High-quality GeSn film was grown epitaxially by MBE on SOI substrates. The Sn content of the GeSn alloy, the mesa diameter, and the absorption-layer thickness were all optimized based on

theory and practical applications. Next, normal-incidence GeSn p-i-n detectors of differing sizes were fabricated by using a CMOS-compatible technology. The 18-μm-diameter device exhibits high responsivities of 0.32 and 0.19 A/W at 1550 and 1630 nm, respectively, and is photoresponsive from 1260 to 1700 nm, covering C, L and most of U telecommunication bands. The 3-dB bandwidth of the 18-μm-diameter device is as high as 28 GHz, which is one of the highest bandwidths reported for normal-incidence GeSn photodetectors. Clear open eye diagrams are obtained under zero bias at 1630 nm. These high-bandwidth, high-responsivity, and broad-photoresponse-wavelength photodetectors thus offer significant potential for use in Si-based optical telecommunications. In the subsequent work, the Sn content in GeSn film can be increased and resonant-cavity structure can also be introduced and optimized to improve the responsivity of the device at 2 μm, so that GeSn photodetectors can has a broad application prospect in the emerging 2 μm band.

References

[1] D. Benedikovic *et al.*, "Silicon–germanium receivers for short-wave-infrared optoelectronics and communications," *Nanophotonics*, vol. 10, no. 3, pp. 1059–1079, 2020.

[2] J. Zheng *et al.*, "Recent progress in GeSn growth and GeSn-based photonic devices," *J. Semiconductors*, vol. 39, no. 6, 2018, Art. no. 061006.

[3] T. Pham *et al.*, "Systematic study of Si-based GeSn photodiodes with 2.6 microm detector cutoff for short-wave infrared detection," *Opt Exp.,* vol. 24, no. 5, pp. 4519–4531, Mar. 2016.

[4] H. Tran *et al.*, "Si-based GeSn photodetectors toward mid-infrared imaging applications," *ACS Photon.,* vol. 6, no. 11, pp. 2807–2815, 2019.

[5] G. T. Reed *et al.*, "Silicon-based Ge0.89 Sn0.11 photodetector and light emitter towards mid-infrared applications," in *Proc. SPIE*, vol. 10108, 2017, Art. no. 1010813-1.

[6] F. Yang *et al.*, "Highly enhanced SWIR image sensors based on $Ge_{1-x}Sn_x$–Graphene heterostructure photodetector," *ACS Photon.,* vol. 6, no. 5, pp. 1199–1206, 2019.

[7] X. Y. Li *et al.*, "Design of $Ge_{1-x}Sn_x$-on-Si waveguide photodetectors featuring high-speed high-sensitivity photodetection in the C- to U-bands," *Appl. Opt.,* vol. 59, no. 25, pp. 7646–7651, Sep. 2020.

[8] B. J. Huang, J. H. Lin, H. H. Cheng, and G. E. Chang, "GeSn resonant-cavity-enhanced photodetectors on silicon-on-insulator platforms," *Opt. Lett.*, vol. 43, no. 6, pp. 1215–1218, Mar. 2018.

[9] Z. Liu *et al.*, "48 GHz high-performance Ge-on-SOI photodetector with zero-bias 40 gbps grown by selective epitaxial growth," *J. Lightw. Technol.,* vol. 35, no. 24, pp. 5306–5310, 2017.

[10] C. Li, C. Xue, Z. Liu, B. Cheng, C. Li, and Q. Wang, "High-bandwidth and high-responsivity top-illuminated germanium photodiodes for optical interconnection," *IEEE Trans. Electron Devices,* vol. 60, no. 3, pp. 1183–1187, Mar. 2013.

[11] S. Klinger, M. Berroth, M. Kaschel, M. Oehme, and E. Kasper, "Ge-on-Si p-i-n photodiodes with a 3-dB bandwidth of 49 GHz," *IEEE Photon. Technol. Lett.,* vol. 21, no. 13, pp. 920–922, Jul. 2009.

[12] H. Tran *et al.*, "Systematic study of $Ge_{1-x}Sn_x$ absorption coefficient and refractive index for the device applications of Si-based optoelectronics," *J. Appl. Phys.,* vol. 119, no. 10, 2016, Art. no. 103106.

[13] K. Ye *et al.,* "Absorption coefficients of GeSn extracted from PIN photodetector response," *Solid-State Electron.,* vol. 110, pp. 71–75, 2015.

[14] H. Tran *et al.*, "High performance Ge0.89Sn0.11 photodiodes for low-cost shortwave infrared imaging," *J. Appl. Phys.,* vol. 124, no. 1, 2018, Art. no. 013101.

[15] S. Wirths *et al.*, "Lasing in direct-bandgap GeSn alloy grown on Si," *Nature Photon.,* vol. 9, no. 2, pp. 88–92, 2015.

[16] L. Colace, G. Assanto, D. Fulgoni, and L. Nash, "Near-infrared pin Ge-on-Si photodiodes for silicon integrated receivers," *J. Lightw. Technol.,* vol. 26, no. 16, pp. 2954–2959, 2008.

[17] C. G. Van de Walle, "Band lineups and deformation potentials in the model-solid theory," *Phys. Rev. B,* vol. 39, no. 3, pp. 1871–1883, Jan. 1989.

[18] W.-J. Yin, X.-G. Gong, and S.-H. Wei, "Origin of the unusually large band-gap bowing and the breakdown of the band-edge distribution rule in the SnxGe1−x alloys," *Phys. Rev. B,* vol. 78, no. 16, 2008, Art. no. 161203.

[19] M. Oehme *et al.*, "GeSn-on-Si normal incidence photodetectors with bandwidths more than 40 GHz," *Opt. Exp.,* vol. 22, no. 1, pp. 839–846, Jan. 2014.

[20] Y. Dong *et al.*, "Two-micron-wavelength germanium-tin photodiodes with low dark current and gigahertz bandwidth," *Opt. Exp.,* vol. 25, no. 14, pp. 15818–15827, Jul. 2017.

[21] S. Xu *et al.*, "High-speed photo detection at two-micron-wavelength: Technology enablement by GeSn/Ge multiple-quantum-well photodiode on 300 mm si substrate," *Opt. Exp.,* vol. 27, no. 4, pp. 5798–5813, Feb. 2019.

[22] H. Tran *et al.*, "Study of GeSn Mid-infrared photodetectors for high frequency applications," *Front. Mater.*, vol. 6, 2019, Art. no. 00278.

[23] H. Zhou *et al.*, "Photo detection and modulation from 1,550 to 2,000 nm realized by a GeSn/Ge multiple-quantum-well photodiode on a 300-mm si substrate," *Opt. Exp.,* vol. 28, no. 23, pp. 34772–34786, Nov. 2020.